An Exploratory Investigation of the High Pressure β-V_2O_5 polymorph as 3 V cathode material for Potassium-Ion Battery

Ankush Bhatia[1]*, Jean-Pierre Pereira-Ramos[1], Maria Elena Arroyo y de Dompablo[2], Rita Baddour-Hadjean[1]*

[1]Institut de Chimie et des Matériaux Paris Est (ICMPE), UMR 7182 CNRS-Université Paris Est Créteil, 2 rue Henri Dunant, 94320 Thiais, France

[2]Departamento de Química Inorgánica, Universidad Complutense de Madrid, Madrid 28040, Spain

Corresponding authors: ritabaddour-hadjean@cnrs.fr/ ankush bhatia

Abstract

Electrochemical potassium-ion insertion in high pressure /high temperature (HP/HT) β-V_2O_5 polymorph is examined for the first time. Monoclinic HP/HT β-V_2O_5 delivers a high reversible capacity of 120 mAh g^{-1} at C/20 rate corresponding to the $K_{0.8}V_2O_5$ composition, at an average discharge potential of 3.2 V vs. K^+/K. A good cycling performance is achieved over at least 175 cycles at C/5 rate at room temperature, confirming HP/HT β-V_2O_5 is an efficient host material for K^+ insertion-extraction reaction. First insight into the reversibility of the structural changes upon potassiation is given.

Keywords: high pressure β-V_2O_5, layered structure, K-ion battery, positive electrode

Introduction

Potassium-ion batteries (KIBs) have garnered significant attention in the field of electrochemical energy storage. This is primarily due to the following key factors: the negative standard potential of K^+/K couple (-2.93 V vs. SHE), lower than that of Na^+/Na system resulting in high operating potential of potassium-based cathode materials as compared to sodium-based alternatives, the potassium abundance in the earth's crust which is nearly equivalent to that of sodium resources, and possibility of the reversible (de)intercalation of K-ions into the graphite anode [1, 2]. These advantages have contributed to the growing interest in exploring the potential of KIBs for practical applications in energy storage [3, 4]. However, the large ionic radius of K^+ (K^+ > Na^+ > Li^+, 1.38 > 1.02 > 0.76 Å in terms of ionic radius) and the large volume changes induced by K^+

accommodation have limited practical application. Therefore, the search for suitable cathode materials remains a crucial challenge in unlocking the full potential of KIBs.

There is ample space available for the exploration and advancement of K-ion cathode materials, with a specific emphasis on layered oxides. The rich redox chemistry of vanadium has led to important interest in V_2O_5 owing to its high theoretical capacity for metal-ion batteries [5]. Variety of K-containing V-based oxides (KVO) such as electroformed $K_xV_2O_5$ ($0 < x < 0.6$) obtained from α-V_2O_5 in potassiated-dimethylsulfone electrolyte at 150°C [6], bilayered δ-$K_{0.5}V_2O_5$ [7], $K_{0.83}V_2O_5$ chemically synthesized by soft chemistry [8] and some hydrated phases such as V_2O_5.0.6-0.8H_2O [9, 10], $K_{0.42}V_2O_5$.0.25H_2O [11] have been reported as promising cathode materials for KIBs. High specific energy and excellent cycling stability make also V-based polyanionic and Prussian blue analogues attractive cathode materials for K storage [3,12–14]. However, only a few papers have focused on the K-storage properties of α-V_2O_5 at room temperature (RT) in standard organic based-electrolytes. Q. Fu *et al*.,[15] in 2021 reported the potassium insertion in orthorhombic nanosized α-V_2O_5 prepared by hydrothermal route. An initial potassiation/depotassiation capacity of 200 $mAhg^{-1}$ (1.36 K^+ ions) at a low potential of 1.7 V vs. K^+/K was displayed with a rapid capacity decline reaching 54 $mAhg^{-1}$ at the 31st cycle. Further, using specific electrode design, crystalline α-V_2O_5 nanorods@rGO [16] and amorphous α-V_2O_5 @CNT [17] were reported as host material for potassium insertion delivering capacity ranging between 50-200 mAh g^{-1}. However, both of these tailored orthorhombic α-V_2O_5 oxides operate at a low discharge potential of around 1.8 V vs. K^+/K. As a proof of concept, our group has recently extended K^+ insertion to another V_2O_5 polymorph called γ'-V_2O_5 with attractive electrochemical features [18]. A high amount of potassium (up to 0.9 K^+ mol^{-1} in the 4.4 – 1.5 V voltage window) can be electrochemically accommodated between the puckered layers of γ'-V_2O_5 at a high discharge potential of ≈3.3 V vs. K^+/K (twofold higher compared to α-V_2O_5) with a stable specific capacity of ~ 50-60 $mAhg^{-1}$.

Looking at other V_2O_5 polymorphs, a few papers outline the potential interest of the layered high pressure/high temperature (HP/HT) β-V_2O_5 polymorph as host lattice for electrochemical insertion reactions. In 2007, Arroyo-de Dompablo *et al*.,[19] showed promising Li^+ insertion capabilities of the β-V_2O_5 polymorph delivering a first discharge capacity of 240 mAh g^{-1} near 3.2 V vs. Li^+/Li, leading to β- $Li_{1.6}V_2O_5$ with stable cycling behavior over at least 27 cycles in the 4 V – 1 V voltage range. Interestingly, Cordoba *et al*.,[20] recently reported Na^+ insertion in β-V_2O_5 at a high potential of ≈ 3 V vs. Na^+/Na delivering a capacity of 132 mAh g^{-1} (β-$Na_{0.9}V_2O_5$) in the 3.6-2.0 V range. However, due to irreversible phase transformations not yet solved, the specific capacity was reported to decrease continuously in the first few cycles before reaching a stable value of 75 mAh g^{-1} at C/10 rate. Very recently, Trocoli *et al*.,[21] reported an extension of β-V_2O_5 insertion properties to the case of magnesium intercalation. Their study used a combination of several characterization techniques to give evidence for the structural changes associated with the Mg^{2+} (de-) intercalation. A specific capacity of 350 mAh g^{-1} was reported on the first

discharge corresponding to the β-$Mg_{1.2}V_2O_5$ composition, but at a low working potential of ≈ 1.4 V vs. K^+/K pointing a difficult magnesium accommodation probably due to the high charge density of Mg^{2+}. These previous data on lithium, sodium and magnesium insertion in β-V_2O_5 motivated us to explore for the first time the electrochemical potassium intercalation characteristics in this high pressure V_2O_5 polymorph.

Material and methods

β-V_2O_5 was prepared according to the protocol described by Arroyo-De Dompablo et al. [22, 23] by subjecting commercial (Aldrich) α-V_2O_5 at a high pressure of 4 GPa and at temperature of 800°C in a Conac press. After the pressure and temperature were applied for 0.5 h, the vessel was quenched to RT while the pressure was slowly released. The morphology and elemental composition of the obtained black-reddish powder were characterized by scanning electron microscopy (SEM), (Zeiss, Merlin-type microscope) and electron dispersive X- ray spectroscopy (EDS) analysis together with SEM using an accelerating voltage of 10 – 15 kV.

Crystal structures were determined using X-ray diffraction (XRD) as well as Raman spectroscopy. XRD experiments were performed using a Panalytical XPert pro apparatus equipped with a X'Celerator detector and using Co Kα radiation (λKα = 1.789 Å). All the diffraction patterns were collected with a 2θ step of 0.0167°. A He:Ne laser (632.8 nm) was used as the excitation source to record the Raman spectra with a LaBRAM HR 800 (Jobin-Yvon-Horiba).

Without any further cathode optimization, 80 wt. % of β-V_2O_5 powder was used to prepare the working electrode by mixing with 7.5 wt % of acetylene black, 7.5 wt. % of graphite and 5 wt. % of PTFE as binder to make a sheet. This sheet was cut into disc of 0.8 cm in diameter (about 6 mg of active material). Potassium metal was used as counter and reference electrode. The CR2032 two electrode coin-cells were assembled in an argon-filled glove box. The positive electrode (sheet) is separated from the negative electrode (K-metal) by Whatman glass fiber disks soaked in 0.5 M KPF_6/Ethylene carbonate (EC): Propylene carbonate (PC) 1:1 2% vol. Fluoroethylene carbonate (FEC) electrolyte. Electrochemical tests were carried out at RT using a VMP3 Biologic apparatus. The cells were electrochemically cycled at different c-rates (C/100-1C).

The XRD patterns and Raman spectra of electrochemically formed β-$K_xV_2O_5$ samples have been recorded according to the following *ex situ* procedure. After 2 hours of equilibrium time, the positive electrodes were removed from the cell in an Ar-filled glove box, rinsed with DMC, and placed in appropriate airtight sample holders to be analyzed by XRD, using a 2θ step of 0.0167° and Raman spectroscopy. Raman spectra were recorded on 10 different spots of each electrode. Similar spectra were recovered for all the investigated points, whatever the electrode, indicating their good homogeneity.

Results and discussion

Figure 1a illustrates the morphology of the as-synthesized powder, which consists of tiny platelets of a few hundred nanometers width. The XRD pattern (**figure 1b)** indicates that pure β-V_2O_5 is obtained with *P21/m* monoclinic symmetry and unit cell parameters *a* = 7.1016(3) Å, *b* = 3.5668(1) Å, *c* = 6.2742(3) Å and *β* = 90.121(3) °, in good agreement with the layered crystal structure proposed by V. P. Filonenko and Gallardo-Amores and illustrated in **Figure 1c** [22-24].

The Raman spectrum of the as-prepared powder (**figure 1d)** exhibits a series of well-resolved bands assigned to a well-crystallized β-V_2O_5 sample, in good agreement with that previously reported [25]. The point group symmetry of β-V_2O_5 is C_{2h}, and therefore, the crystallographic sites of V, O_1 and O_2 atoms split into two nonequivalent positions distinguished by subscripts a and b in **Figure S1.** The crystal structure of β-V_2O_5 is built up of [V_2O_5] units forming infinite chains along the *y* direction. The chains are linked by corner-sharing octahedra forming layers held together by relatively weak interactions and stacked along the *x* direction. Three types of V-O bonds can be identified in the units (**Figure S1**) [25]: the shortest vanadyl V-O_1 bonds, V-O_3 bonds forming asymmetric V-O_3-V bridges in the *xz* plane and V-O_2 bonds forming V-O_2-V bridges oriented along the *y* direction. Based on the results of calculations, the Raman peaks of pristine β-V_2O_5 have been previously assigned to specific vibrational modes taking into account these structural data. The two sharp peaks at 1017 and 937 cm^{-1} are assigned to the stretching modes of the shortest V_a-O_{1a} and V_b-O_{1b} bonds, respectively. Then, the vibrations of the bridging O_3 atoms give rise to the V_b-O_3 and V_a-O_3 stretching modes observed at 739 and 583 cm^{-1}, respectively. The Raman line at 682 cm^{-1} corresponds to the asymmetric vibration of O_{2a} atoms in the V_a-O_{2a}-V_b bridge while the band at 472 cm^{-1} is attributed to the stretching of the V_b-O_{2a} bond. Below 450 cm^{-1}, several well-resolved peaks are observed, which are mostly assigned to complex vibrations of the V_2O_5 chains.

Figure 2a shows the cyclic voltammogram (CV) of β-V_2O_5 recorded in the 2.2 – 4.4 V vs. K^+/K voltage range at a sweeping rate of 0.1 mV s^{-1}. CV curves show two broad cathodic peaks centered at ca. 3.04 V and 2.4 V with a shoulder at 2.84 V and four anodic peaks centered at ca. 3.08 V, 3.48 V, 3.84 V and 4.15 V. Such observations suggest the participation of different structural mechanisms involved during the reduction and oxidation processes. Noteworthy, the same coulombic charge was involved during reduction and oxidation, showing the high efficiency of the electrochemical process. It can be noticed a slight shift in the cathodic peak potentials (~100 mV) between cycle 1 and 2 showing an easier potassium insertion process induced after a first reduction-oxidation cycle.

In order to get a quasi-equilibrium potential evolution vs. K composition in the electrode, a galvanostatic discharge-charge curve of β-V_2O_5 electrode was carried out at a low rate of C/100 (~1.5 mA g^{-1}) in the 2.2 – 4.4 V voltage range (**Figure 2b)**. Three well-defined insertion

steps at 3.4 V, 3.0 V and 2.7 V are clearly evidenced. The first discharge plateau at 3.4 V involves a potassium uptake of 0.32 corresponding to a capacity of 47 mAh g^{-1}, and then it is followed by a sloping curve from 3.25 V to 2.7 V with additional 0.28 inserted K^+ ions (41 mAh g^{-1}). The last step observed as a flat voltage plateau at 2.7 V involves a potassium uptake of 0.26 K^+ corresponding of a further capacity of 40 mAh g^{-1}. The total discharge capacity involved in the reduction process is ~127 mAh g^{-1}, leading to a composition of $K_{0.85}V_2O_5$ for the discharged product. The subsequent charge process includes 4 steps at 2.8 V, 3.5 V, 3.9 V and 4.2 V with a total capacity of 130 mAh g^{-1}. This first discharge-charge cycle displays a coulombic efficiency of around 100%. Such results indicate that different mechanisms are probably involved during K^+ insertion and deinsertion, ensuring however a high rechargeability. **Figure 2b** clearly shows the interest provided by the structure of β-V_2O_5 as host lattice for K insertion since the redox process occurs between 3.48 and 2.2 V vs. K^+/K, i.e. ≈ 3.28 V-2.V vs. Na^+/Na, which corresponds to the same potential range and potential insertion steps previously reported for sodium ions [20]. This result shows that the expected penalty due to the size effect is not observed for potassium accommodation, at least from a thermodynamic point of view. Interestingly, the size effect (or more precisely, the polarizing capability) of the inserted cation seems to be vital if one compares Na/K with Li. As reported by Gallardo el al [19], Li intercalation proceeds throughout six fully reversible reduction/oxidation steps in a wide voltage range (4.2-1 V).

Rate capability tests in the C/20 to 1C range confirm the promising performance of β-V_2O_5 electrode. The first discharge-charge cycle of the β-V_2O_5 electrode at different current densities is shown in **figure 2c**. A galvanostatic cycle recorded at C/20 rate reveals a discharge capacity of 120 mAh g^{-1} at an average discharge potential of 3.1 V. **Table 1** shows the results of EDS analysis of the discharged electrodes recovered at two different lower cut off potential (2.6 V and 2.2 V) performed at a C/20 rate. The K/V ratio found from EDS measurements were 0.25 (discharge till 2.6 V) and 0.40 (discharge till 2.2V), which is consistent with the compositions of $K_{0.54}V_2O_5$ and $K_{0.82}V_2O_5$, respectively. A subsequent charge capacity of 118 mAh g^{-1} was obtained with a coulombic efficiency of 99%. The EDS analysis of the charged electrode gives a K/V ratio of 0.05 ($K_{0.1}V_2O_5$), which is close to the potassium content calculated from the faradaic yield (0.06 F mol^{-1}). The difference between the remaining amounts of K^+ ions can be explained by a less efficient rinsing procedure for this particular experiment. A strong influence of the current density is observed in the C/20 –C/5 range, suggesting a kinetically hindered intercalation reaction. This is probably due to the slow diffusion of large sized potassium-ion (ionic radius of 1.38 Å). Indeed, a capacity of 120 mAh g^{-1} is reached at C/20 (~8 mA g^{-1}), 85 mAh g^{-1} at C/10 (~16 mA g^{-1}), 60-65 mAh g^{-1} at C/5 (~32 mA g^{-1}) and C/2 (~80 mA g^{-1}), respectively, with still 50 mAh g^{-1} obtained at 1C (~160 mA g^{-1}). These results are very close or higher than those reported for sodiation with capacities of 130, 80 and 75 mAh g^{-1} at respectively C/20, C/10 and C/5 and only ~ 10 mAh g^{-1} at 1C [20].

The above rate capability study confirms the attractive properties of β-V_2O_5. Regarding other K-cathode materials, β-V_2O_5 well competes with γ'-V_2O_5 [18] and K_xMnO_2/$K_xMn_{0.75}Ni_{0.25}O_2$ [26]. The maximum capacity of 120 mAh g^{-1} displayed by β-V_2O_5 significantly exceeds that exhibited by some bilayered potassium bronzes like $K_{0.5}V_2O_5$ [7] and $K_{0.83}V_2O_5$ [8] and is equal to that offered by the best KVO compound, i. e. $K_{0.5}V_2O_5$ [27], the latter being characterized by a better rate capability.

Galvanostatic cycling experiments of β-V_2O_5 composite electrode was also performed at a C/10 rate (~16 mA g^{-1}) in the same 4.4 V – 2.2 V potential window. As shown in **figure 3a**, starting from the OCV voltage of 3.87 V vs. K^+/K, the voltage quickly falls down to ~3.22 V, then follows a gentle slope till 2.6 V trailing by a second plateau starting at 2.6 V till 2.2 V. A total discharge capacity of c.a. 85 mAh g^{-1} (0.58 F mol^{-1}) is then reached at 2.2 V. Upon subsequent charge of the cell, four steps at 2.9 V, 3.6 V, 4.0 V and 4.35 V are observed involving a total capacity of 71 mAh g^{-1} indicating a coulombic efficiency of 84%. A small amount of 0.1 K^+ is probably trapped after the first charge. However, on the second cycle, the same discharge/charge capacities of 85 mAh g^{-1} are observed, indicating a quantitative charge process. In addition, potassiation of β-V_2O_5 seems to be easier since occurring ~100mV higher than in the first cycle (3.1 V vs. K^+/K). Further discharge-charge cycles completely superimpose till 5th cycle (**figure 3b)**. The different voltage steps in both charge and discharge become less marked, resulting in a reversible S-shape profile with a mid-discharge potential of around 3.2 V. Surprisingly, the width of the second plateau between 2.6 and 2.2 V gradually diminishes with the cycling and completely disappears from the 10th cycle. This suggests that fewer phase transformations take place upon charge/discharge. Additional analysis of the structural changes is required to understand the underlying cause for this phenomenon.

Figure 3c illustrates the specific discharge capacities of β-V_2O_5 in K cells as a function of the cycle number when cycled at different current densities. The discharge capacity decreases rapidly from 120 mAh g^{-1} from the first cycle at C/20 till 20th cycle to reach a stable capacity of 65 mAh g^{-1} at 30th cycle. Notably when cycled at C/10 rate, a stable capacity of 52 mAh g^{-1} is involved over 120 cycles and still 43 $mAhg^{-1}$ are recovered after 175 cycles at C/5 rate. At both C/2 and 1C rate, a lower capacity of 35 $mAhg^{-1}$ is achieved after 100 cycles. The present cycling data show the capacity fading mainly comes from the last step contribution located at 2.5 V at C/10 rate. **Figure S2** shows that by changing the lower cut off voltage from 2.2 V to 2.6 V (to avoid the last insertion step), a better cycling behaviour is obtained. Indeed, the huge capacity fading over the first ten cycles is suppressed. The capacity slowly decreases from 60 to 50 mAh g^{-1} after 40 cycles and remains stable at least up to cycle 80. These results serve as a proof of the extraordinary structural stability exhibited by the β-V_2O_5 material upon K^+ successive insertion/deinsertion processes, as observed in the case of lithiation [19] but differently from what was reported in the case of sodiation [20].

For comparison, the electrochemical behavior at RT of the conventional micrometric sized α-V_2O_5 polymorph has also been investigated at C/10 rate in the same 4.4 V – 2.2 V potential window, using the same KPF_6 EC: PC electrolyte (**figure S3**). The corresponding cycling behaviour of α-V_2O_5 is reported in **figure 3c and figure S3**. In this case, a reversible capacity of only 4 mAh g^{-1} is reached at 2.2 V, corresponding to the $K_{0.04}V_2O_5$ composition, indicating that practically no redox activity occurs upon potassium insertion in micrometric sized α-V_2O_5 polymorph. In the case of ~~a~~ nanosized α-V_2O_5, [15] a discharge capacity of 45 $mAhg^{-1}$ was reported at 2.2 V vs. K^+/K while the major redox activity was observed at very low voltage of around 1.75 V.

These findings support the remarkable ability of the β-V_2O_5 structure to accommodate K^+ ions at a high energy level (3.2 V vs. K^+/K), which is much higher (+1.45 V) than that observed in the case of nanosized α-V_2O_5, showing a much easier insertion process. Furthermore, a twofold specific discharge capacity is reached in the same voltage range. The superior electrode characteristics of the β-V_2O_5 polymorph compared to the ambient pressure polymorph have been previously discussed [22,23]. The electrical conductivity of the electrode material is crucial for the kinetics of the intercalation reaction, therefore governing the polarization of the positive electrode and the power rate capability of the lithium cell. To the best of our knowledge there are no reports comparatively investigating the ionic conductivity in the layered structures of the two polymorphs. Regarding the electronic conductivity, the measured resistivities at room temperature are 10.000 Ωcm in α-polymorph vs. 400 Ω cm in the β-polymorph [22]. The enhanced electronic conductivity of HP-V_2O_5 with respect to that of the ambient pressure form is a major advantage in terms of electrochemical performance.

A deep structural investigation is required for understanding the electrochemical properties of β-V_2O_5 and in particular the structural pathways for the phase transformations upon discharge and charge as well as the crucial role of the last step at 2.6 V on the cycling behaviour.

A first insight into the structural changes occurring in β-V_2O_5 upon potassium insertion can be given by analyzing the ex-situ XRD patterns and Raman spectra recorded at the end of the first discharge at 2.2 V (corresponding to $K_{0.8}V_2O_5$ composition), after first charge and 120^{th} charge (**Figures 4 and 5, respectively**). Upon the first reduction (0.8 K), a significant shift of the (*100*) diffraction peak to lower angles is observed (**Fig. 4**), which is associated with an elongation in the *a* axis from 7.1 to ~ 9 Å induced by K^+ insertion in the interlayer space. A similar phenomenon was reported to take place for Mg [21] and in a larger extent for Na [20] insertion (*a* = 10.097 Å for 0.7 Na). Upon the first oxidation, most of the reflections of β-V_2O_5 are recovered with however the disappearance of the lowest angle (*100*) peak and a broadening of the lines suggesting some amorphization upon K^+ deinsertion. This disordering process is all the more marked after 120 discharge-charge

cycles but the structure of β-V_2O_5 seems to be retained, which account for the good cycling stability evidenced above.

Raman spectroscopy experiments reveal also significant changes upon the first K ion insertion (first discharge, see **Fig. 5**): Indeed, the bands in the low frequency region are still visible but become weak and broad, suggesting a disordered character in spite of the retaining of the local structure of the chains when moving from β-V_2O_5 to $K_{0.8}V_2O_5$. The high frequency band features undergo significant intensity and frequency variation. The 1017 cm^{-1} peak assigned to the vibration of the terminal V_a-O_{1a} bond disappears while an intense new band appears at 890 cm^{-1} with a shoulder at 855 cm^{-1}. Two new components are also seen in the region corresponding to the vibrations of the bridging O_3 atoms at 772 and 527 cm^{-1}. These observations are consistent with K ions insertion in the interlayer space of V_2O_5 impacting the V-O bonding in the vicinity of the terminal O_{1a} and bridging O_3 atoms while O_{2a} /O_{2b} atoms vibrations located in the chains are little affected (**Figure S1**). The important frequency shift of the V_a-O_{1a} vibration ($\Delta\nu$ = -130 cm^{-1}) suggests a significant lengthening of this bond upon K insertion. After the first cycle, it is remarkable to observe again the Raman fingerprint of the pristine material with only slight alteration in the high frequency region. This comment is also true when looking at the Raman spectra after 10 and 120 cycles, showing the structural reversibility at the atomic scale of the transformation upon several K insertion-deinsertion reactions.

These preliminary ex-situ structural characterization reveal an overall reversible K^+ insertion/extraction process, that leads back to the pristine phase. This contrasts with the irreversible potassiation process previously reported in the case of nanosized α-V_2O_5 [15]. Work is in progress to elucidate the detailed mechanism of K^+ intercalation/deintercalation in HP-V_2O_5.

Conclusion

Reversible potassium insertion into layered β-V_2O_5 host is reported here for the first time. Phase-pure β-V_2O_5 is synthesized by subjecting commercial α-V_2O_5 at a high pressure and temperature. Potassium ion intercalation properties of monoclinic type β-V_2O_5 structure are confirmed by EDS, XRD and Raman analyses. β-V_2O_5 polymorph shows reversible K-ion deinsertion involving multiple stepwise voltage profiles leading to a discharge capacity of 120 mAh g^{-1} at C/20 rate corresponding to the $K_{0.8}V_2O_5$ composition at a mid-discharge potential of 3.2 V vs. K^+/K. The β-V_2O_5 system overpasses the parent α-V_2O_5 phase in terms of specific capacity and working voltage and competes with the γ'-V_2O_5 polymorph and the best bilayered KVO [27]. Preliminary cycling tests show stable capacities of 60 and 50 mAh g^{-1} at C/20 and C/10 respectively over tens of cycles. However, further studies are required to understand the structural changes and the K^+ diffusion process in β-V_2O_5 in order to improve its rate capability and cycling properties. As a result, β-V_2O_5 can be proposed as a suitable host material for K-ion insertion with superior performance than the parent α-V_2O_5.

This study confirms once more the richness of polymorphism in the V_2O_5 system in terms of insertion properties and electrochemical behavior.

Table 1. K/V ratios in different electrodes from EDS analysis and Electrochemistry (EC).

Electrode History	F/mol	x in $K_xV_2O_5$ (EC)	K/V ratio (EDS)	x in $K_xV_2O_5$ (EDS)
1st Discharge till 2.6 V (C/20)	0.54	0.54	0.25	0.5
1st Discharge till 2.2 V (C/20)	0.82	0.82	0.40	0.80
1st Charge till 4.4 V after D-2.2 V (C/20)	0.06	0.06	0.053	0.1

References

[1] W. Luo, J. Wan, B. Ozdemir, W. Bao, Y. Chen, J. Dai, L. Hu, (2015). "Potassium ion batteries with graphitic materials," Nano Lett. 15, 7671–7677. https://doi.org/10.1021/acs.nanolett.5b03667

[2] S. Komaba, T. Hasegawa, M. Dahbi, K. Kubota, Potassium intercalation into graphite to realize high-voltage/high-power potassium-ion batteries and potassium-ion capacitors, Electrochem. Commun. 60 (2015) 172–175. https://doi.org/10.1016/j.elecom.2015.09.002.

[3] T. Hosaka, K. Kubota, A.S. Hameed, S. Komaba, Research Development on K-Ion Batteries, Chem. Rev. 120 (2020) 6358–6466. https://doi.org/10.1021/acs.chemrev.9b00463.

[4] H. Kim, J.C. Kim, M. Bianchini, D.H. Seo, J. Rodriguez-Garcia, G. Ceder, Recent Progress and Perspective in Electrode Materials for K-Ion Batteries, Adv. Energy Mater. 8 (2018) 1–19. https://doi.org/10.1002/aenm.201702384.

[5] X. Xu, F. Xiong, J. Meng, X. Wang, C. Niu, Q. An, L. Mai, Vanadium-Based Nanomaterials: A Promising Family for Emerging Metal-Ion Batteries, Adv. Funct. Mater. 30 (2020) 1–36. https://doi.org/10.1002/adfm.201904398.

[6] J.P. Pereira-Ramos, R. Messina, J. Perichon, Electrochemical Formation of Vanadium Pentoxide Bronzes $M_xV_2O_5$ in Molten Dimethylsulfone, J. Electrochem. Soc. 135 (1988) 3050–3057. https://doi.org/10.1149/1.2095486.

[7] L. Deng, X. Niu, G. Ma, Z. Yang, L. Zeng, Y. Zhu, L. Guo, Layered Potassium Vanadate $K_{0.5}V_2O_5$ as a Cathode Material for Nonaqueous Potassium Ion Batteries, Adv. Funct. Mater. 28 (2018) 1800670. https://doi.org/10.1002/adfm.201800670.

[8] Y. Zhang, X. Niu, L. Tan, L. Deng, S. Jin, L. Zeng, H. Xu, Y. Zhu, $K_{0.83}V_2O_5$: A New Layered Compound as a Stable Cathode Material for Potassium-Ion Batteries, ACS Appl. Mater. Interfaces. 12 (2020) 9332–9340. https://doi.org/10.1021/acsami.9b22087.

[9] X. Liu, G.A. Elia, X. Gao, B. Qin, H. Zhang, S. Passerini, Highly Concentrated KTFSI : Glyme Electrolytes for K/Bilayered-V_2O_5 Batteries, Batter. Supercaps. 3 (2020) 261–267. https://doi.org/10.1002/batt.202000003.

[10] B. Tian, W. Tang, C. Su, Y. Li, Reticular V 2 O 5 ·0.6H 2 O Xerogel as Cathode for Rechargeable Potassium Ion Batteries, ACS Appl. Mater. Interfaces. 10 (2018) 642–650. https://doi.org/10.1021/acsami.7b15407.

[11] M. Clites, J.L. Hart, M.L. Taheri, E. Pomerantseva, Chemically Preintercalated Bilayered $K_xV_2O_5$ n H_2O Nanobelts as a High-Performing Cathode Material for K-Ion Batteries, ACS Energy Lett. 3 (2018) 562–567. https://doi.org/10.1021/acsenergylett.7b01278.

[12] A. Eftekhari, Potassium secondary cell based on Prussian blue cathode, J. Power Sources. 126 (2004) 221–228. https://doi.org/10.1016/j.jpowsour.2003.08.007.

[13] X. Jiang, T. Zhang, L. Yang, G. Li, J.Y. Lee, A Fe/Mn-Based Prussian Blue Analogue as a K-Rich Cathode Material for Potassium-Ion Batteries, ChemElectroChem. 4 (2017) 2237–2242. https://doi.org/10.1002/celc.201700410.

[14] K. Chihara, A. Katogi, K. Kubota, S. Komaba, $KVPO_4$ F and $KVOPO_4$ toward 4 volt-class potassium-ion batteries, Chem. Commun. 53 (2017) 5208–5211. https://doi.org/10.1039/C6CC10280H.

[15] Q. Fu, A. Sarapulova, L. Zhu, G. Melinte, A. Missyul, E. Welter, X. Luo, M. Knapp, H. Ehrenberg, S. Dsoke, In operando study of orthorhombic V_2O_5 as positive electrode materials for K-ion batteries, J. Energy Chem. 62 (2021) 627–636. https://doi.org/10.1016/j.jechem.2021.04.027.

[16] P. Vishnuprakash, C. Nithya, M. Premalatha, Exploration of V_2O_5 nanorod@rGO heterostructure as potential cathode material for potassium-ion batteries, Electrochim. Acta. 309 (2019) 234–241. https://doi.org/10.1016/j.electacta.2019.04.092.

[17] F. Ye, D. Lu, X. Gui, T. Wang, X. Zhuang, W. Luo, Y. Huang, Atomic layer deposition of core-shell structured V_2O_5@CNT sponge as cathode for potassium ion batteries, J. Mater. 5 (2019) 344–349. https://doi.org/10.1016/j.jmat.2018.05.009.

[18] A. Bhatia, J.-P. Pereira-Ramos, N. Emery, R. Baddour-Hadjean, γ'-V_2O_5 Polymorph as a Promising Host Structure for Potassium Storage: an Electrochemical and Structural Study, Chem. Mater. 33 (2021) 5276–5289. https://doi.org/10.1021/ACS.CHEMMATER.1C01390.

[19] M.E. Arroyo y de Dompablo, J.M. Gallardo-Amores, U. Amador, E. Morán, Are high pressure materials suitable for electrochemical applications? HP-V_2O_5 as a novel electrode material for Li batteries, Electrochem. Commun. 9 (2007) 1305–1310. https://doi.org/10.1016/j.elecom.2007.01.035.

[20] R. Córdoba, A. Kuhn, J.C. Pérez-Flores, E. Morán, J.M. Gallardo-Amores, F. García-Alvarado, Sodium insertion in high pressure β-V_2O_5: A new high capacity cathode material for sodium ion batteries, J. Power Sources. 422 (2019) 42–48. https://doi.org/10.1016/j.jpowsour.2019.03.018.

[21] R. Trócoli, P. Parajuli, C. Frontera, A.P. Black, G.C.B. Alexander, I. Roy, M.E. Arroyo-De Dompablo, R.F. Klie, J. Cabana, M.R. Palacín, β-V_2O_5 as Magnesium Intercalation Cathode, ACS Appl. Energy Mater. 5 (2022) 11964–11969. https://doi.org/10.1021/acsaem.2c02371.

[22] J.M. Gallardo-Amores, N. Biskup, U. Amador, K. Persson, G. Ceder, E. Morán, M.E. Arroyo y de Dompablo, Computational and Experimental Investigation of the

Transformation of V_2O_5 Under Pressure, Chem. Mater. 19 (2007) 5262–5271. https://doi.org/10.1021/cm071360p.

[23] M.E.A. Dompablo, U. Amador, J.M. Gallardo-Amores, C. Baehtz, N. Biskup, E. Morán, High pressure materials for energy storage: the case of V_2O_5, J. Phys. Conf. Ser. 121 (2008) 032001. https://doi.org/10.1088/1742-6596/121/3/032001.

[24] V.P. Filonenko, M. Sundberg, P.E. Werner, I.P. Zibrov, Structure of a high-pressure phase of vanadium pentoxide, β-V_2O_5, Acta Crystallogr. Sect. B Struct. Sci. 60 (2004) 375–381. https://doi.org/10.1107/S0108768104012881.

[25] R. Baddour-Hadjean, M.B. Smirnov, K.S. Smirnov, V.Y. Kazimirov, J.M. Gallardo-Amores, U. Amador, M.E. Arroyo-De Dompablo, J.P. Pereira-Ramos, Lattice dynamics of β-V_2O_5: Raman spectroscopic insight into the atomistic structure of a high-pressure vanadium pentoxide polymorph, Inorg. Chem. 51 (2012) 3194–3201. https://doi.org/10.1021/ic202651b.

[26] A. Bhatia, J.P. Pereira-Ramos, N. Emery, B. Laïk, R.I. Smith, R. Baddour-Hadjean, An Exploratory Investigation of Spinel $LiMn_{1.5}Ni_{0.5}O_4$ as Cathode Material for Potassium-Ion Battery, ChemElectroChem. (2020) 1–10. https://doi.org/10.1002/celc.202000889.

[27] Y-H. Zhu, Q. Zhang, X. Yang, E-Y. Zhao, T. Sun, X-B. Zhang, S. Wang, X-Q. Yu, J-M. Yan, Q. Jiang, Reconstructed Orthorhombic V_2O_5 Polyhedra for Fast Ion Diffusion in K-Ion Batteries, Chem., 5 (2019) 168-179. https://doi.org/10.1016/j.chempr.2018.10.004

Figure captions

Figure 1. Characterization of the as prepared β-V_2O_5 powder (a) SEM image; (b) X-ray diffraction pattern; (c) Schematic structural representation in the xz projection; (d) Raman spectrum.

Figure 2. Electrochemical performance of β-V_2O_5 (a) CV curves at 0.1 mV s^{-1}; (b) First discharge-charge cycle at C/100 rate; (c) First discharge-charge cycle at different C-rates. 2.2-4.4 V voltage window. 0.5M KPF_6 EC: PC + 2% FEC electrolyte.

Figure 3. Electrochemical performance of β-V_2O_5 (a) First and second discharge-charge cycles at C/10 rate; (b) Discharge-charge cycles from cycle 1 to 120 at C/10 rate; (c) Evolution of the specific capacity upon cycling at different C-rates. 2.2-4.4 V voltage window. 0.5M KPF_6 EC: PC + 2% FEC electrolyte.

Figure 4. XRD patterns of the pristine electrode, after first discharge till 2.2 V leading to $K_{0.8}V_2O_5$ composition (red), after first discharge-charge cycle (green) and after 120 cycles (black). *: PTFE reflection. G: Graphite line.

Figure 5. Raman spectra of the initial electrode, after first discharge till 2.2 V leading to $K_{0.8}V_2O_5$ composition (red), after first discharge-charge cycle (green), after 10 cycles (blue) and after 120 cycles (black).

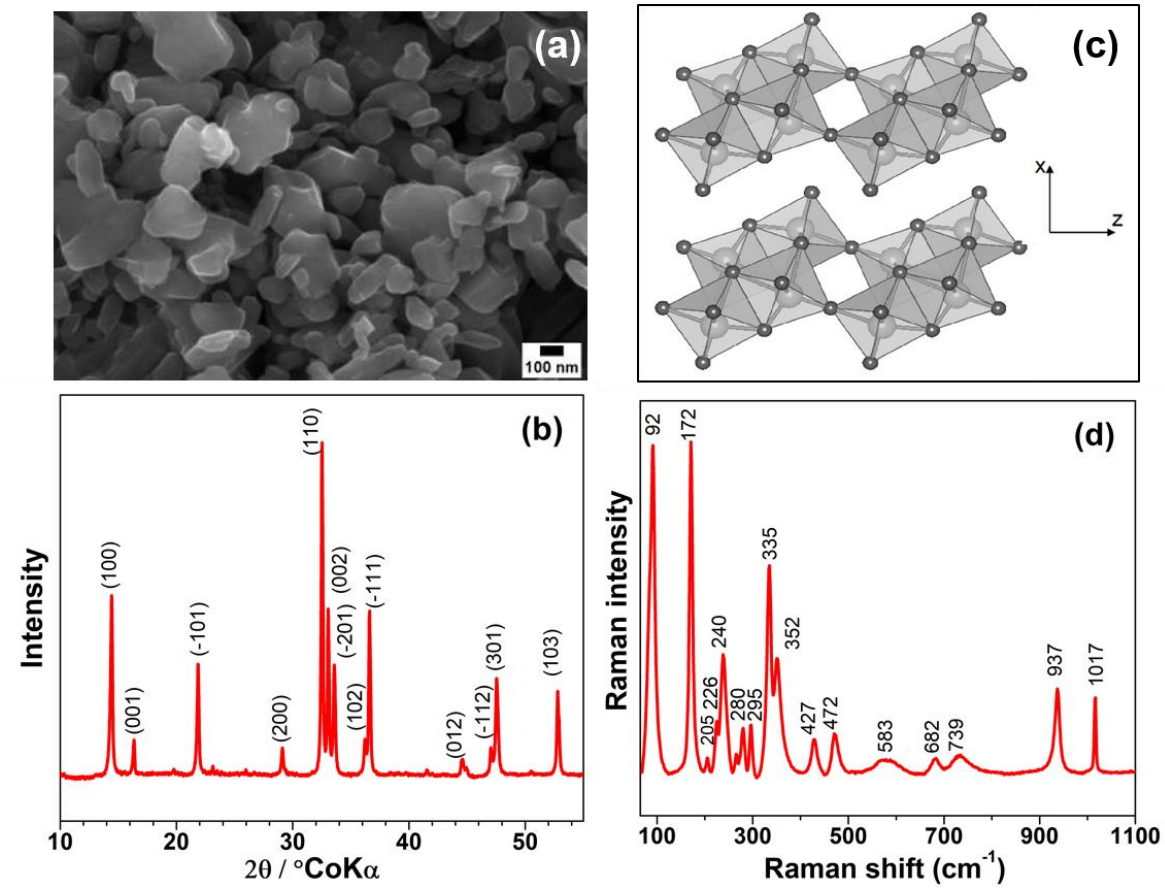
(a)
100 nm
(c)
X
Z
(b)
Intensity
(100)
(001)
(-101)
(200)
(110)
(002)
(-201)
(102)
(-111)
(012)
(-112)
(301)
(103)
10
20
30
40
50
2θ / °CoKα
(d)
Raman intensity
92
172
205
226
240
280
295
335
352
427
472
583
682
739
937
1017
100
300
500
700
900
1100
Raman shift (cm-1)

Figure 1

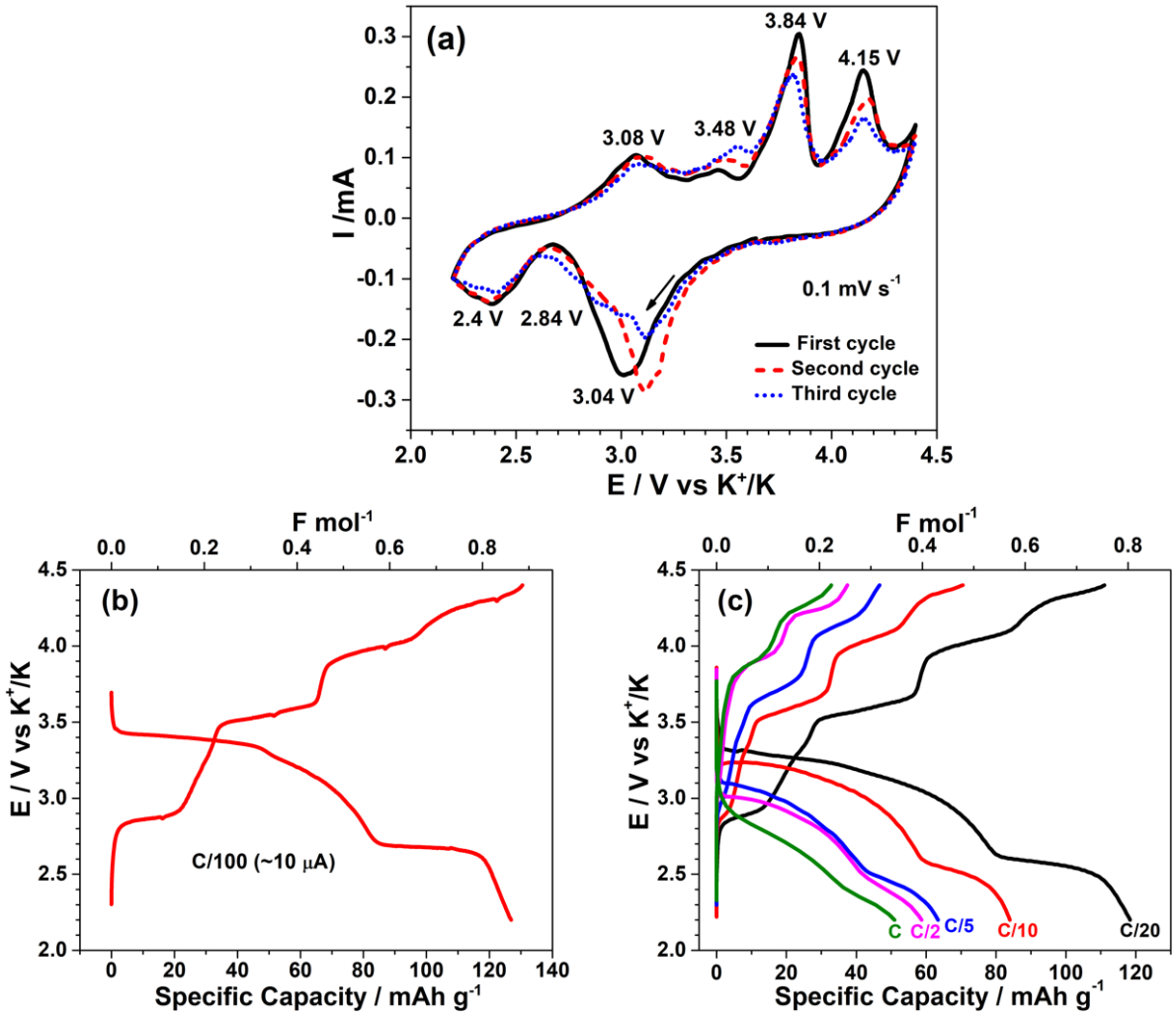
(a)
3.84 V
4.15 V
3.08 V
3.48 V
2.4 V
2.84 V
3.04 V
0.1 mV s-1
First cycle
Second cycle
Third cycle
I /mA
E / V vs K+/K
(b)
C/100 (~10 μA)
F mol-1
E / V vs K+/K
Specific Capacity / mAh g-1
(c)
C
C/2
C/5
C/10
C/20
F mol-1
E / V vs K+/K
Specific Capacity / mAh g-1

Figure 2

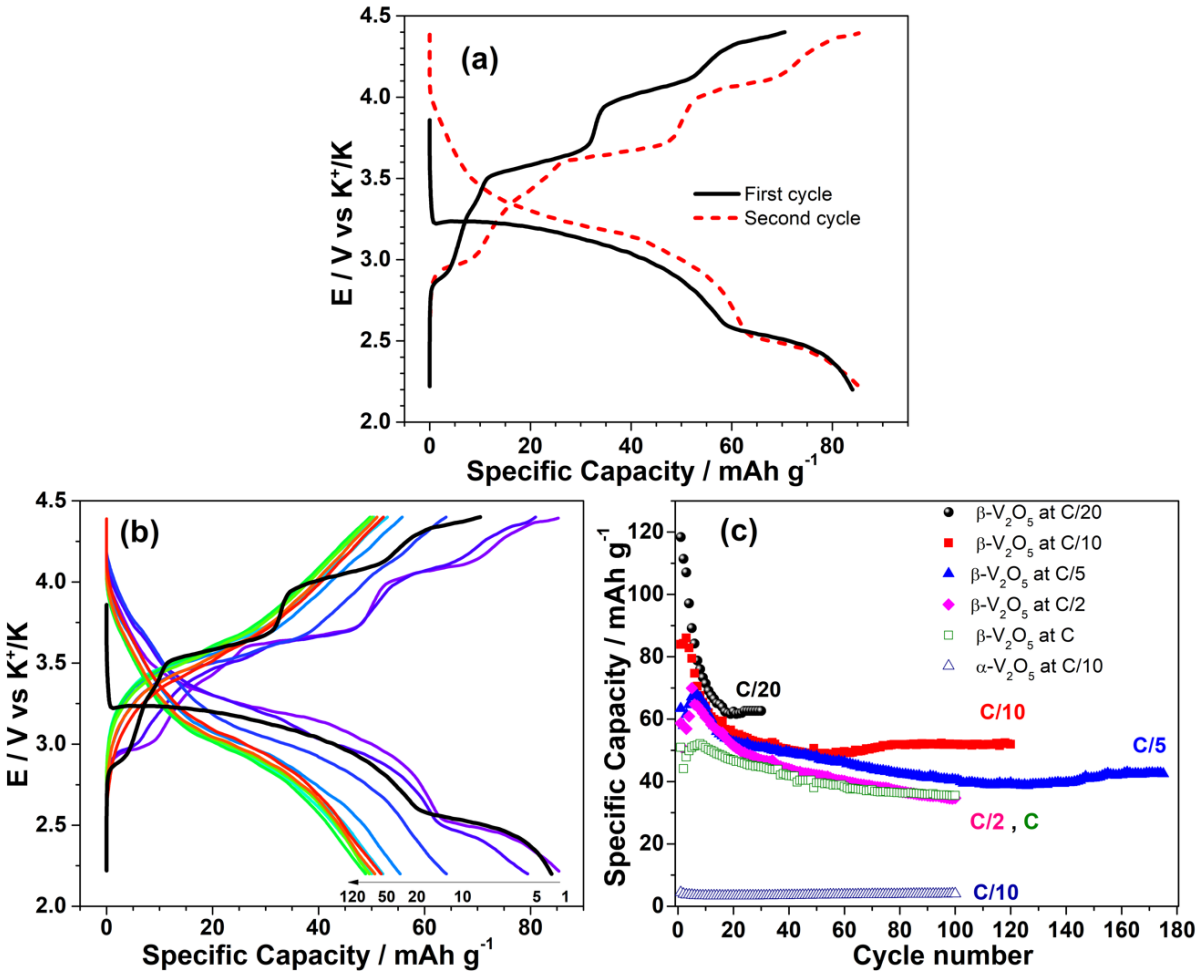
(a)
First cycle
Second cycle
E / V vs K+/K
Specific Capacity / mAh g-1
(b)
120 50 20 10 5 1
E / V vs K+/K
Specific Capacity / mAh g-1
(c)
β-V2O5 at C/20
β-V2O5 at C/10
β-V2O5 at C/5
β-V2O5 at C/2
β-V2O5 at C
α-V2O5 at C/10
C/20
C/10
C/5
C/2 , C
C/10
Specific Capacity / mAh g-1
Cycle number

Figure 3

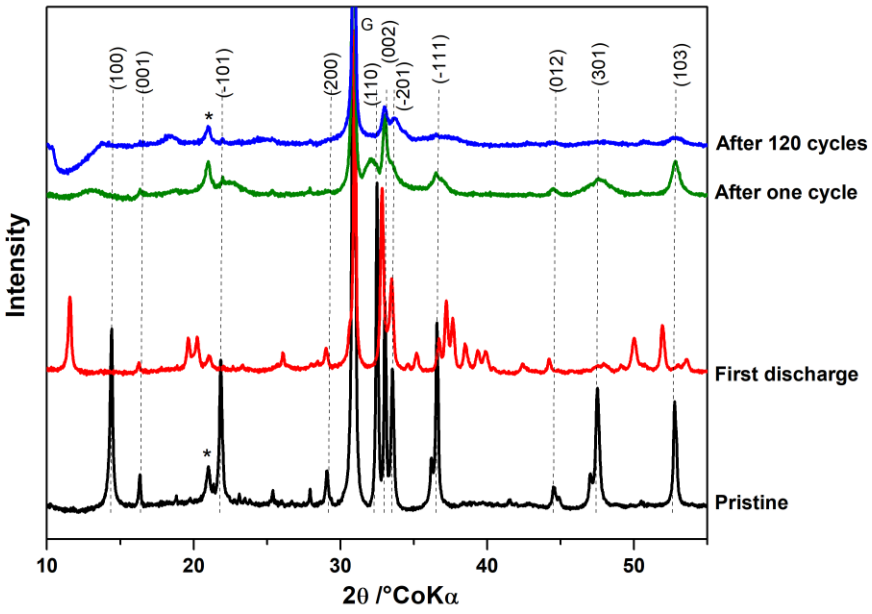

Figure 4 (revised)

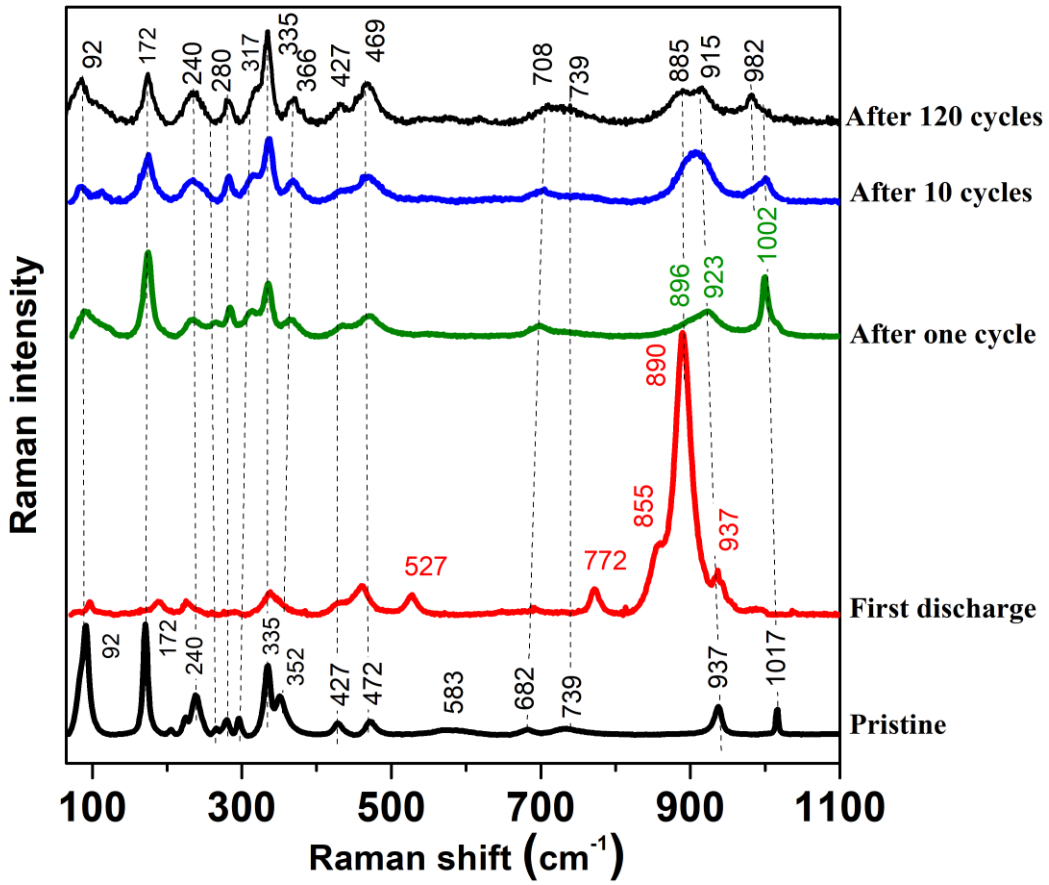
Raman intensity
Raman shift (cm-1)
100
300
500
700
900
1100
After 120 cycles
After 10 cycles
After one cycle
First discharge
Pristine
92
172
240
280
317
335
366
427
469
708
739
885
915
982
1002
896
923
890
855
937
527
772
352
472
583
682
1017

Figure 5